J Sol-Gel Sci Technol (2010) 53:316–321
DOI 10.1007/s10971-009-2094-z

ORIGINAL PAPER

Synthesis of fluorine doped tin oxide nanoparticles by sol–gel technique and their characterization

V. Senthilkumar · P. Vickraman · R. Ravikumar

Received: 18 June 2009 / Accepted: 7 October 2009 / Published online: 27 October 2009

Abstract This article presents novel attempt to synthesis of fluorine doped tin oxide (FTO) nanoparticles by sol–gel technique. The synthesized FTO nanoparticles were obtained after calcination. Temperatures of calcination were 600 and 700 °C due to identify changes in the particles size growth. A DG/DTA and FTIR study identifies the oxide and formation of the nanopowders. The XRD studies confirm the tetragonal crystallite structure of fluorine doped tin oxide. The TEM image confirms the size of FTO particles in nanoscale. The electrical studies on FTO nanopowders results the decrease in resistivity profile with increasing calcinations. The optical band gap studies for sol–gel synthesis FTO nanoparticles is found to be in the range of 4.11–3.84 eV conforming decreasing optical band gap with increasing calcinating temperatures.

Keywords FTO · Nanopowder · Sol–gel · XRD · TEM · Optical band gap

1 Introduction

The miniscule gate ways of ultrafine particles have yielded very exciting microscopic properties in contrast to the macroscopic entities. In other words, nanometer size of the particles revolutionize the material science particularly oxide materials towards their new applications in optoelectronic, electrochromic, lithium battery technologies and so on.

When the vision of the nanoparticles world maneuvers with the sizes of the particles as it encompasses the physical properties of the materials, many new properties appeared for particles diameter below 100 nm. The number of atoms in the particle surface becomes comparable to the number of atoms inside the particle that exemplifying the very remarkable physical properties as their completely deviating from the changing bonding geometry of the bulky materials. Sensationally, the size effects which yielded reduced brittleness and improve ductility for structured ceramic materials are observed. Provoking the particle size is smaller than 20 nm in diameter. Its realized that the requisite temperature for melting and sintering reduces below 30% with reference to that of the bulky materials are very noteworthy phenomena in the material science processing [1].

The sparkling size of sprouting nanosized materials have brought into the technological revolution rather reflected in their optical, electrical and magnetic properties. For example, SnO_2 which is promising and dominant technically provoking the semiconducting material's world. With their wide band gap of 3.6 eV its transport mechanism is not dependent on the stoichiometry rather which emancipates its sensory functions with their oxygen vacancies in the SnO_2 lattice [2]. The conductivity of the undoped SnO_2 limited to 10^2–10^3 Ω^{-1} cm^{-1} spurs the high dependency on the oxygen vacancies in the latch of the lattice [3–6]. This inherent abnormality opens the new gateways of doping SnO_2 with some elements such as Sb, F, and Mo to make SnO_2 as a very compatible material for engulfing very many windows of semiconductor applications such as displays, electrochromic windows, gas sensors, catalysts, rechargeable Li batteries, and optical electronic devices [7, 8].

V. Senthilkumar · P. Vickraman (✉)
Department of Physics, Gandhigram Rural University, Gandhigram 624302, India
e-mail: vrsvickraman@yahoo.com

R. Ravikumar
Electrochemical and Power Source Division, Central Electrochemical Research Institute, Karaikudi, India

The doping of fluorine to SnO_2 is primarily concentrated to promote to have more number of charge carriers there by leading to achieve enhanced electrical conductivity rather to the expected optimum value of $\sim 5 \times 10^3\ \Omega^{-1}\ cm^{-1}$, for an optimum atomic F/Sn ratio of $\sim 3\%$ [9].

The immense applications of gas sensors are interlinked with their electrical resistance. The electrical resistance is mainly relaying upon their crystallite resistance i.e., within a crystallite as a distance from its surface increases which is dependent on the ratio of the electron concentration to that in air, the sensitivity of the gas sensor increases with the decrease in crystallite size [10]. In this line it has been demonstrated that sensitivity of nanocrystalline based gas sensors increases dramatically as a size of the SnO_2 decreases. For example, it has been demonstrated that the gas sensitivity of nanocrystalline SnO_2 sensors increases drastically as the size of SnO_2 crystallites decreases below ~ 10 nm [11]. In the field of lithium-ion battery, very small tin oxide particles are needed to obtain high capacity [12], which requires the preparation of nanosized SnO2 particles. Up to now, tin oxide nanoparticles are prepared by different synthesis methods, such as sol–gel synthesis [13], sonochemical method [14], hydrothermal method [15], laser decomposition reaction [16], and solid state reaction [17]. The sol–gel method is one of the most promising available methods for synthesizing nanoparticles of controlled size and morphology. So, this method is adopted and applied to the synthesis F-doped SnO_2 nanocrystalline powders [18, 19] in the present study.

2 Experimental procedure

The Fluorine doped Tin oxide nanocrystalline powders were prepared by sol–gel techniques. The starting chemicals of high purity $SnCl_2{\cdot}2H_2O$ (analytical reagent) and HF 50% were used for preparation fluorine doped tin oxide (FTO) nanopowders. For the synthesis FTO nanopowder, 25 g of SnCl*H_2O and 1.85 g of 50% HF solution were dissolved in 500 mL deionized water. The mixed solution was slowly added to a solution of 25 mL acetylacetone in 70 mL methanol with rapid stirring. The addition acetylacetone solution took about 45 min, while the rapid stirring was continued. The aqueous ammonia solution was added to the mixed solution by drop wise until to get gel formation. The dropping rate must be well controlled (the optimum pH value of solution is 9.5) to obtain the chemical homogeneity. The resulting gel product was filtered and washed several times with cold water till removal of the entire Cl^- ions before being transferred to the oven for further drying at 100 °C. The absent of Cl^- ions was checked by 0.1 N $AgNO_3$ solution. Dried material converted to alcogel by methanol, and nanopowders of FTO were obtained in furnace by calcination in duration of 2 h at 600 and 700 °C, respectively.

2.1 Characterization

Differential thermal analysis (DTA) and thermo gravimetry (TA Instruments-SDT Q600) of prepared precursors were carried out from room temperature to 1,000 °C, in the heating rate of 20 °C min^{-1} and in dynamic air atmosphere. Fourier transform infrared spectroscopy (FT-IR) analysis (Thermo Nicolet Nexus 670) was undertaken to confirm the oxide and the residual organic moieties in the sample. The structural properties of the as-deposited and calcined powders were studied by X-ray diffractometer (PANalytical-X'pert pro, Cu Kα1 radiation at $\lambda = 0.15418$ nm) in the 2θ range 10–80°. The Transmission electron micrograph (TEM) images were taken with FEI-Tecnai 20 G^2 transmission electron microscope. The samples for the TEM were prepared by ultrasonically dispersing the product in acetone, and then droplets were placed on carbon coated Cu grids. Diffuse reflectance Spectra (DRS) were recorded using VARIAN Carry 500 UV–VIS spectrophotometer.

3 Results and discussion

Differential thermal analysis is carried out to examine the conversion process of the precursors during calcinations. Figure 1 shows the profile of weight loss of precursor as a function of temperature, as measured by DGA. The DGA profile shows that the precursor is subjected to gradual weight loss in the temperature spectrum of 30–600 °C, and showing a marked slow weight loss beyond 600 °C. The maximum weight loss rate observed around 100 °C is

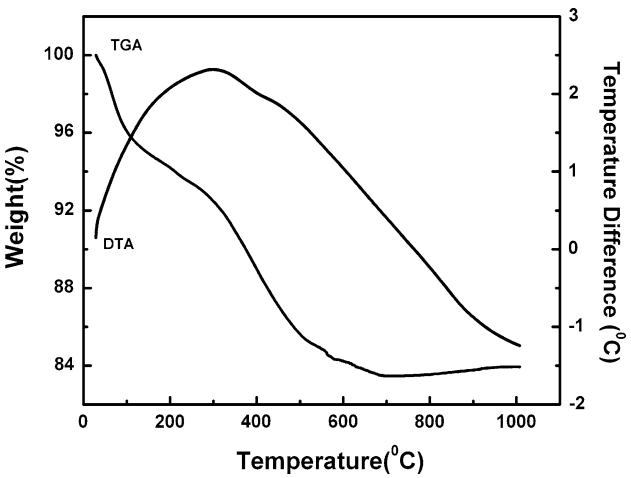

Fig. 1 TG, DTA curves for the decomposition of FTO precursor at a heating rate of 20 °C min^{-1} under a dynamic atmosphere of air

related with the release of water and chemisorbed methanol on the surface of the precursor powders. The DTA thermal event recorded gradual exothermic trend throughout the entire thermal range of the system. This supplements with TGA data and means that precursor is transformed into oxide particles around 600 °C as shown in TGA curve. Thus thermal study provides sample temperature profile consequently it is realized to fix the calcining temperature at 600 °C to study the perfect decomposition.

Figure 2 shows the FTIR spectrum of the Fluorine doped tin oxide nanopowders prepared at room temperature (RT) and calcined at 600 and 700 °C for 2 h in air by sol–gel technique. The Fig. 2a shows very distinct sharp vibrational bands at 656 and 561 cm^{-1} are attributed to Sn–O–Sn and Sn–O (belonging to Sn–OH groups) stretching vibrations, respectively [20]. 880The fundamental characteristic vibrational band at 561 cm^{-1} corresponds to Sn–O stretching shifts towards the higher wavelength side one at 626 cm^{-1} and another one at 667 cm^{-1}, respectively for 600 and 700 °C calcinating temperatures revealing the information about the complete removal of organic residuals in FTO nanopowders. The broad absorption in the frequency band 2,500–3,750 cm^{-1} and sharp absorption band at 1,630 cm^{-1} in the higher frequency region are assigned to the O–H stretching from residual alcohol, water, and SnO–H bonds [21]. The sharp adsorption at 1,630 cm^{-1} is associated with the deformation vibration of H–O–H bonds of the physisorbed water. The FT-IR spectrum confirms that some hydroxyl groups still remain, even in the samples calcined at higher temperatures as shown in Fig. 2b, c [22].

Figure 3a illustrates the XRD spectra of fluorine doped SnO_2 powders as synthesized and calcinated for 2 h at 600 and 700 °C. The spectra identify the presence of SnO_2 only and the peaks associated with fluorine could not be detected. It reveals that fluorine might have been incorporated into the crystal lattice of SnO_2 via the sol–gel process. The presence of fluorine in SnO_2 lattice was

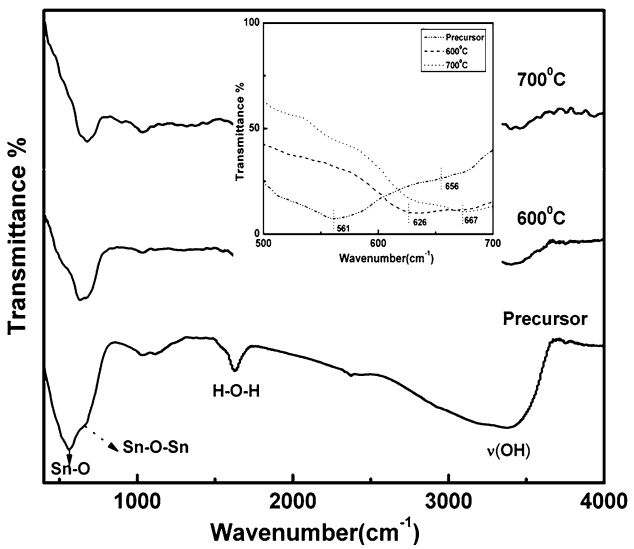

Fig. 2 FT-IR spectra of Fluorine doped SnO_2 nanopwdres. The *inset* shows the FT-IR spectrum in the range 700–500 cm^{-1}

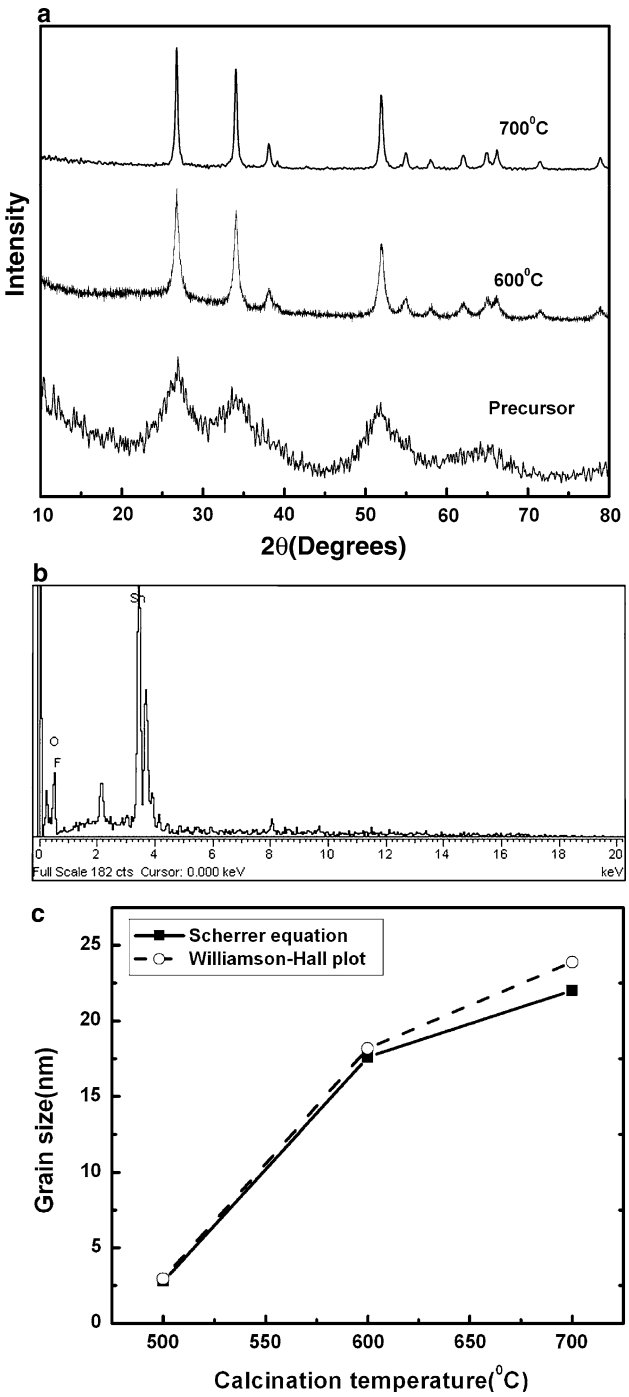

Fig. 3 **a** XRD patterns of fluorine doped SnO_2 nanoparticles with different calcination temperatures; **b** EDAX spectrum of the FTO nanopowders calcinated at 600 °C, **c** different calcinations temperatures verses Particle sizes of the FTO nanoparticles were calculated using Sherrer and Williamson–Hall plot

confirmed from the EDAX spectrum (see Fig. 3b). All diffraction lines are well assigned to tetragonal crystallite phases of tin oxide (with the reference pattern JCPDS 880287). From Fig. 3, it is noted that the intensity of the SnO_2 peaks increases with increasing calcinations temperature and the full-width half-maximum (FWHM) widths of the peaks decreases with increasing temperature as well indicates that crystallization of the SnO_2 powders progresses gradually as the treating temperature increases(see Fig. 3c). The experimental data show that crystallization of the SnO_2 gel is not completed at a temperature of 100 °C, but perfect crystals could be obtained at higher treating temperatures at 600 and 700 °C.

The FWHM's can be expressed as a linear combination of the contributions from the strain and particle size by the following equation [23]

$$\beta\cos\theta = \frac{k\lambda}{L} + \eta\sin\theta$$

where λ the wavelength of the X-rays, θ is the diffraction angle, η is the lattice strain, L is the crystallite size, k is a constant (0.94), and β is the full width at half maximum (FWHM). Figure 4a represents the plot of $\beta\cos\theta/\lambda$ against $\sin\theta/\lambda$. Slope of the graph depicts strain values which lies in the range 3.5×10^{-2}–3.24×10^{-4} and the intercept on y-axis gives the crystallite size which lie in the range 2.96–23.88 nm. It is clear from the strain results that as the calcining temperature increases, the particle size also increases whereas the strain value decreases (see in Fig. 4b).

Figure 5a, b illustrates the TEM image and SAED patterns of fluorine doped tin oxide nanoparticles calcined at 600 °C for 2 h. The close examination of the size of FTO particles reveals that it falls in nano-scale, and these particles from Fig. 5a are found to be agglomerated. In general, agglomeration occurs in the case of nanoparticles very easily because the surface forces such as Vander-Waals forces, capillary forces and electrostatic forces could overcome only against gravitational and inertial forces for particles in this size range [24]. The average diameter of particles is evaluated to be approximately 15–17 nm. The results of grain size measurement from TEM observation

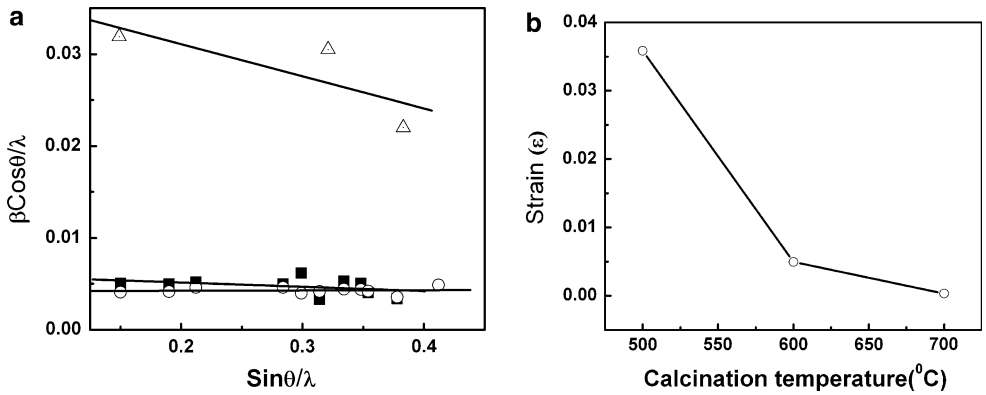

Fig. 4 **a** Williamson–Hall plot of SnO_2 nanopowder doped with fluorine; **b** variation of strain with calcinations temperature

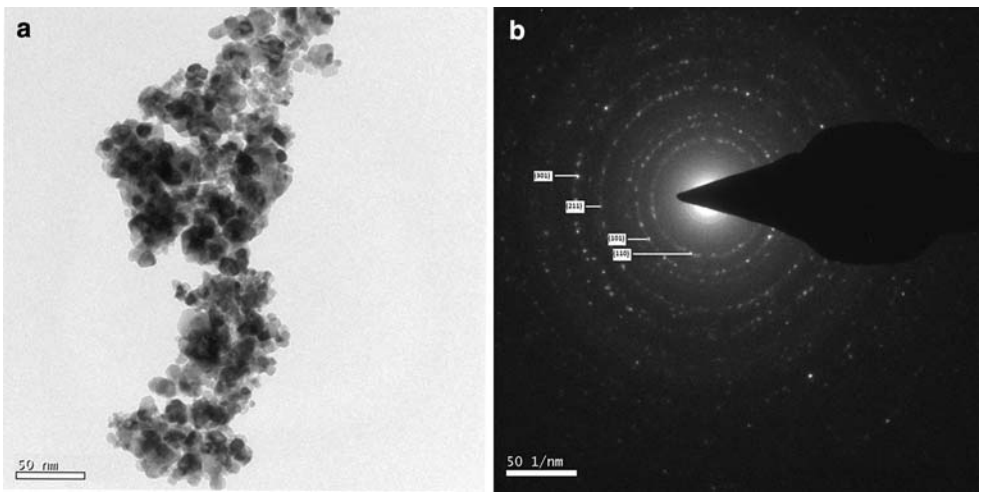

Fig. 5 **a**, **b** TEM image and SAED patterns of FTO nano particles calcined at 600 °C for 2 h

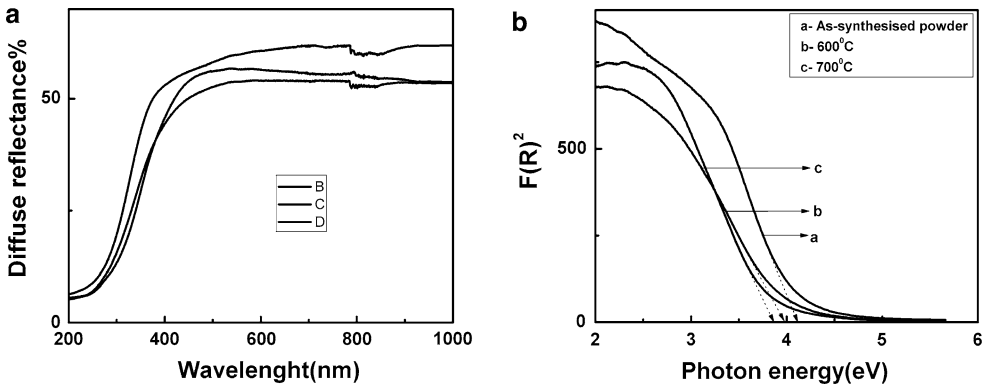

Fig. 6 **a** The diffuse reflectance spectra results of FTO nanopowders and **b** plots of $F(R)^2$ vs photon energy of SnO_2 nanopowders

are having good agreement with the X-ray line broadening method. The *d* spacing values calculated from SAED pattern for well reflected planes (110),(101),(211) and (301) were found respectively to be 0.332, 0.262, 0.173, and 0.139 nm . These obtained values were agreed with the bulk values.

The resistivity was calculated for all Fluorine doped SnO_2 nanoparticles. The FTO nanopowders were pressed to a circular pellet of 7 mm diameter under 5 ton pressure for 2 min by using hydraulic pelletizer, and inserting the pellet between two rods of brass and the resistance was observed. The resistivity was calculated by using the formula $\rho = RA/d$ where 'ρ' is resistivity R is the actual resistance, A is the cross section area of circular pellet, and d is the pellet thickness. The measured values of the resistivity for as prepared and calcinated at 600 and 700 °C were found to be 3.7, 4.27, and 4.61×10^{-4} Ω cm, respectively.

Figure 6a illustrates the diffuse reflectance spectra of the sol–gel synthesized fluorine doped tin oxide nanopowders. The band gap of FTO nanopowders could be determined on the basis of the following relation for direct band gap semiconductors [25]

$$\alpha\alpha(hv - Eg)^{1/2}$$

where α is the absorption coefficient, hv is the photon energy and Eg is the band gap. The absorption coefficient α is related to reflectance R by

$$\alpha = SF(R)/2v_p$$

where S is the scattering coefficient, v_p is the volume fraction of the absorbing species and $F(R)$ is Kubelka–Munk function, in which R is the experimentally observed reflectance:

$$F(R) = (1 - R)^2/2R$$

If the dependence of the scattering coefficient S on wavelength of the incident light is neglected, the Kubelka–Munk function is directly proportional to the absorption coefficient

$$\alpha = (S/2v_p)F(R) = \text{con} \times F(R)$$

The purpose of determining the band gap, extrapolating the $F(R)^2$ versus energy curve to $F(R)^2 = 0$ is equivalent to carry out the same procedure with α^2 versus energy curve. A plot of $F(R)^2$ versus photon energy is shown in Fig. 6b. The band gap for sol–gel synthesized FTO nanopowders is determined in the range 4.11–3.84 eV. It is clear that Eg decreases with increasing calcinating temperature and its minimum value of 3.84 eV is obtained at a temperature of 700 °C. The variation of optical band gap corresponds to grain size is reasonably attributed due to the quantum size effect [26].

4 Conclusion

Using sol–gel technique, Fluorine doped nanocrystalline SnO_2 powder has been successfully synthesized. The synthesized FTO nanopowders are analyzed at 600 and 700 °C calcinating temperatures. Oxide phase formation has been found through TG/DTA and also FT-IR studies. X-ray diffraction pattern confirms the tetragonal structure of SnO_2 and identifying absent of fluorine peaks in the XRD spectrum. The change in particle size towards the calcinations shows that the particle size increases with increasing calcinations temperature whereas strain values are decreases. The results of TEM observation for grain size measurement are in good agreement with the X-ray line broadening method. The lower resistivity of 4.61×10^{-4} Ω cm for higher calcinating temperature favours higher conductivity was obtained from electrical studies. The optical band gap values decreases with increasing calcinating temperature due to the quantum size effect.

References

1. Lindackers D, Janzen C, Rellinghaus B, Wassermann EF, Roth P (1998) Nanostruct Mater 10:1247

2. Nutz T, zum Felde U, Haase M (1999) J Chem Phys 110:12142
3. Zhang J, Gao L (2004) Inorg Chem Commun 7:91
4. Shukla S, Ludwig L, Parrish C, Seal S (2005) Sens Actuators B Chem 104:223
5. Sun K, Liu J, Browning ND (2002) J Catal 205:266
6. Santos-Peña J, Brousse T, Sánchez L, Morales J, Schleich DM (2001) J Power Sources 97:232
7. Zhang J, Gao L (2004) Mater Res Bull 39:2249
8. Chandra Bose A, Kalpana D, Thangadurai P, Ramasamy S (2002) J Power Sources 107:138
9. Chopra KL, Major S, Pandya DK (1983) Thin Solid Films 102:1
10. Seal S, Shukla S (2002) J Met 54:35
11. Shukla S, Seal S, Ludwig L, Parish C (2004) Sens Actuators B Chem 97:256
12. Aurbach D, Nimberger A, Markovky B, Levi E, Sominski E, Gedanken A (2002) Chem Mater 14:4155
13. Ansari SG, Boroojerdian P, Kulkarni SK, Sainkar SR, Karekar RN, Aiyer RC (1996) J Mater Sci-Mater El 7:267
14. Zhu J, Lu Z, Aruna ST, Aurbach D, Gedanken A (2000) Chem Mater 12:2557
15. Cheng HM, Ma JM, Zhao ZG, Qi LM (1996) Chem J Chin U17:833
16. Ocaña M, Matijevic E (1990) J Mater Res 5:1083
17. Gao SM, Pang L, Che HW, Zhou XP (2004) China Particul 2:177
18. Boegeat D, Jousseaume B, Toupance T, Campet G, Fournès L (2000) Inorg Chem 39:3924
19. Gamard A, Jousseaume B, Toupance T, Campet G (1999) Inorg Chem 38:4671
20. Xiong H-M, Zhao K-K, Zhao X, Wang Y-W, Chen J-S (2003) Solid State Ionics 159:89
21. Epifani M (2001) J Am Ceram Soc 84:48
22. Kersen Ü, Sundberg MR (2003) J Electrochem Soc 150:H129
23. Tan ST, Chen BJ, Sun XW, Fan WJ, Kwok HS, Zhang XH, Chua SJ (2005) J Appl Phys 98:013505
24. Pugh RJ, Bergström L (1994) Surface and colloid chemistry in advanced ceramic processing. Marcel Dekker, New York, p 273
25. Kortum G (1969) Reflectance spectroscopy. Springer, New York
26. Zhu H, Yang D, Yu G, Zhang H, Yao K (2006) Nanotechnology 17:2386